Mon. Not. R. Astron. Soc. **383,** L5–L9 (2008) doi:10.1111/j.1745-3933.2007.00399.x

Mixing in massive stellar mergers

E. Gaburov,[1,2]★ J. C. Lombardi, Jr[3] and S. Portegies Zwart[1,2]

[1]*Sterrenkundig Instituut 'Anton Pannekoek', University of Amsterdam, the Netherlands*
[2]*Section Computational Science, University of Amsterdam, the Netherlands*
[3]*Department of Physics, Allegheny College, 520 North Main Street, Meadville, PA 16335, USA*

Accepted 2007 September 21. Received 2007 September 21; in original form 2007 July 20

ABSTRACT

The early evolution of dense star clusters is possibly dominated by close interactions between stars, and physical collisions between stars may occur quite frequently. Simulating a stellar collision event can be an intensive numerical task, as detailed calculations of this process require hydrodynamic simulations in three dimensions. We present a computationally inexpensive method in which we approximate the merger process, including shock heating, hydrodynamic mixing and mass loss, with a simple algorithm based on conservation laws and a basic qualitative understanding of the hydrodynamics of stellar mergers. The algorithm relies on Archimedes' principle to dictate the distribution of the fluid in the stable equilibrium situation. We calibrate and apply the method to mergers of massive stars, as these are expected to occur in young and dense star clusters. We find that without the effects of microscopic mixing, the temperature and chemical composition profiles in a collision product can become double-valued functions of enclosed mass. Such an unphysical situation is mended by simulating microscopic mixing as a post-collision effect. In this way we find that head-on collisions between stars of the same spectral type result in substantial mixing, while mergers between stars of different spectral type, such as type B and O stars ($\sim$10 and $\sim$40 $M_\odot$ respectively), are subject to relatively little hydrodynamic mixing. Our algorithm has been implemented in an easy-to-use software package, which we have made publicly available for download.[1]

Key words: hydrodynamics – molecular processes – shock waves – methods: numerical – blue stragglers – stars: general.

1 INTRODUCTION

The cores of star clusters can become so dense that close encounters and even collisions between stars become quite common (Portegies Zwart et al. 1999). This effect is particularly important in young star clusters where a broad range of stellar masses dominates the dynamical evolution of the cluster core. In a star cluster with an initial half-mass relaxation time smaller than a few tens of million years, core collapse can occur well before the most massive stars leave the main sequence and explode in a supernova. In such star clusters, these massive stars will dominate the core dynamics. This is most noticeable in both the arrest of core collapse by the formation of tight massive binaries and the occurrence of physical collisions between stars which are mediated by the binaries (Gaburov, Gualandris & Portegies Zwart 2007).

Simulating stellar collisions in globular clusters has attracted considerable attention over the last decade. These calculations were mainly initiated to explain the presence and characteristics of blue stragglers (Sills et al. 2002; Lombardi et al. 2002; Lombardi, Rasio & Shapiro 1996). In many cases, collisions occur infrequently enough that the already computationally expensive dynamical modelling of a cluster would hardly be slowed down by a simple treatment of collisions. However, it was recently recognized that the number of collisions in young star clusters can become quite large, and this may lead to formation of a very massive object (Portegies Zwart et al. 2004; Freitag, Gürkan & Rasio 2006). Furthermore, the subsequent evolution of such objects, and of collision products in general, can depend on their internal structure.

To determine the structure of a collision product accurately, one can resort to high-resolution numerical simulations of stellar mergers. Such simulations are generally carried out by means of the smoothed particle hydrodynamics (SPH) method (Monaghan 2005). This however becomes computationally expensive, especially if one is interested in multiple collisions which may occur in the course of *N*-body simulations. On the other hand, components of multiple systems, such as binaries and triples, may experience a collision (Gaburov et al. 2007), and careful treatment of such collisions might play an important role for further evolution of these multiple systems. Therefore, faster methods are needed to compute the outcome of a stellar merger event, and these methods can eventually be included in *N*-body simulations.

Lombardi et al. (1996) constructed a method which has been successfully used for collisions between low-mass main-sequence stars, and in this Letter we extend this method to collisions between massive stars. Our method has a general applicability, in the sense that it is suitable for mergers of all stellar types, including compact objects.

★E-mail: egaburov@science.uva.nl
[1]http://www.astro.uva.nl/∼egaburov/mmas2

2 METHODS

2.1 Guiding principle

The guiding idea of our method is Archimedes' principle. To determine how fluid will redistribute itself when brought out of equilibrium, perhaps by a stellar merger, we need to consider densities: a fluid element with a greater density than its environment will accelerate downward, while one with a smaller density will be buoyed upward. Any such element can ultimately settle into hydrostatic equilibrium once its density equals that of its environment. The density of a fluid element will not in general remain constant during the collision. Instead, it will be continuously adjusted in such a way that pressure equilibrium with the environment is achieved. In other words, parcels of gas expand or contract as necessary to equilibrate their pressure with the environment.

We begin by considering a distribution of gas, in our case stars, and specify distribution functions for the pressure P, density ρ and abundance of chemical species X_i as a function of the enclosed mass. For a given equation of state, the expression for the entropy can be determined. It is often mathematically simpler, although not formally necessary, to define an entropic variable A which is related to the specific entropy and conserved by fluid elements in adiabatic processes; we call this entropy variable A the buoyancy.

The buoyancy can be calculated from the equation of state, $P = P(A, \rho, X_i)$. In the case of an ideal gas $A = P/\rho^{\Gamma}$, where Γ is the adiabatic index. By construction, the buoyancy A depends directly upon entropy and composition, and it remains constant for each fluid element in the absence of heating and mixing. Therefore, it is an important starting point for understanding the hydrodynamics of collisions.

This idea has been successfully used to describe the underlying hydrodynamics of collisions among low-mass main-sequence stars (Lombardi et al. 1996, 2002, 2003), which are well described by a monatomic ideal gas equation of state. In this case $\rho = (P/A)^{3/5}$, such that at a given pressure, a smaller A yields a greater value of ρ. Consequently, fluid with smaller values of A sink to the bottom of a potential well, and the A profile of a star in stable hydrostatic equilibrium increases radially outwards. Indeed, it is straightforward to show that the condition $\mathrm{d}A/\mathrm{d}m > 0$ is equivalent to the usual Ledoux criterion for convective stability of a non-rotating star (Lombardi et al. 1996).

2.2 Sorting algorithm

The fluid in high-mass main-sequence stars is well described by a mixture of monatomic ideal gas and radiation in thermal equilibrium. In such cases, the total pressure is

$$P = \frac{\rho k T}{\mu} + \frac{a T^4}{3}, \tag{1}$$

where k is the Boltzmann constant, T is temperature, μ is the mean molecular mass and a is the radiation constant. The specific entropy is (Clayton 1983)

$$s - s_0 = \frac{3}{2}\frac{k}{\mu}\left[\log\left(\frac{kT}{\rho^{2/3}\mu}\right) + \frac{8}{3}\frac{1-\beta}{\beta}\right] \equiv \frac{3}{2}\frac{k}{\mu}\log A, \tag{2}$$

where the quantity s_0 depends only on composition and β is the ratio of gas to total pressure. To achieve the equality in equation (2), we define the buoyancy A through the following relation

$$P = \frac{A\rho^{5/3}}{\beta}\mathrm{e}^{-\frac{8}{3}\frac{1-\beta}{\beta}}. \tag{3}$$

Through manipulations with equations (1), (2) and (3) and definition of β, we find

$$\rho = \frac{3k^4}{A^3\mu^4 a}\frac{1-\beta}{\beta}\mathrm{e}^{8\frac{1-\beta}{\beta}}. \tag{4}$$

Together, equations (3) and (4) provide the desired relationships between the pressure, buoyancy, density and composition. Given a prescription for shock heating and an estimate of the mass loss, it is possible to determine the structure of a non-rotating product resulting from a head-on collision of two massive main-sequence stars, which we call parent stars.

To begin with, we consider fluid elements at the centre of each parent star and determine which one will settle in the centre of the collision product. For this purpose, we both make an initial estimate of the central pressure of the collision product and test which fluid element would have larger density when brought to this central pressure: a process that can be completed in two steps. First, as the composition and post-shock buoyancy of each fluid element can be considered known, equation (3) gives what would be the final β value of each element if it were to settle at the centre of the collision product. Secondly, these β values correspond to densities through equation (4). The fluid element with the greater density is the one that actually settles in the centre of the collision product. Next, we integrate the equations of hydrostatic equilibrium to determine the local pressure P throughout the product. This local pressure is used to determine which of subsequent fluid elements from the parent stars contribute to the structure of the product. This procedure is repeated until the mass supply of the parent stars is depleted. As in the case of low-mass main-sequence stellar collisions, the central pressure is iteratively improved until the outer boundary condition, namely that the surface pressure vanishes, is satisfied.

As a consequence of this merging procedure, one must expect that fluid of a certain composition that has originated in one parent star can be located arbitrarily close to fluid of a different composition from the other parent. These fluid elements must be in pressure equilibrium and also, by the condition of hydrostatic equilibrium, have the same density. Therefore, in order to have adjacent fluid elements of different μ, equations (3) and (4) imply that these elements must have different buoyancies A. We therefore should not expect that the A and μ profiles in a nascent collision product will be single-valued, at least not before mixing has occurred on the microscopic level.

If the parent stars have essentially the same homogeneous composition as in the merger of two unevolved stars, then μ will be uniform throughout the collision product, and for any given pressure, greater densities will correspond to smaller values of the buoyancy. In other words, the structure of the collision product can then be simply determined by sorting the fluid in order of increasing A: the lowest A fluid is placed at the centre of the product and is surrounded by shells with increasingly higher values of A. The merging procedure also reduces to sorting by A in another special case, namely when radiation pressure is negligible ($\beta \to 1$), as equation (3) clearly reduces to the monatomic ideal gas result in this limit. The merging procedure presented here is therefore a natural generalization of that presented for low-mass stars in Lombardi et al. (2002, 2003).

2.3 Stability criterion in high-mass Stars

The unusual profiles that can be achieved in stellar mergers suggest that we take a careful look at the condition for convective stability:

$$\left(\frac{\mathrm{d}\rho}{\mathrm{d}r}\right)_{\mathrm{env}} < \left(\frac{\mathrm{d}\rho}{\mathrm{d}r}\right)_{\mathrm{el}}. \tag{5}$$

Table 1. The simulations carried out in this work. The model name of the simulations are given in the first column. The masses of the primary and the secondary stars are shown in the second and the third column respectively. The evolutionary state of the parent stars is given in the fourth column: TAMS, HAMS, and ZAMS stand for turn-off age, half-age and zero-age main sequence respectively. In the fifth column we show the number of SPH particles in the simulations; in all cases, we use well over 100 k equal-mass SPH particles in order to achieve high resolution in the dense stellar interiors and to insure convergent results.

Model	M_1	M_2	Evolutionary state	N
T88, H88	80	8	TAMS, HAMS	880k
T48, H48	40	8	TAMS, HAMS	480k
T28, H28, Z28	20	8	TAMS, HAMS, ZAMS	280k
T18, H18, Z18	10	8	TAMS, HAMS, ZAMS	180k

Here, the subscripts 'env' and 'el' refer to the environment and the fluid element, respectively. As pressure equilibrium between the element and its immediate environment is established nearly instantaneously, the condition for convective stability can be written in the following way:

$$\left(\frac{\mathrm{d}\log P}{\mathrm{d}\log\rho}\right)_{\rm env} < \left(\frac{\mathrm{d}\log P}{\mathrm{d}\log\rho}\right)_{\rm el}. \quad (6)$$

Using equations (3) and (4), we evaluate derivatives on both sides of equation (6). We then note that

$$\Gamma_1 = \frac{-3\beta^2 - 24\beta + 32}{24 - 21\beta} = \frac{5}{3} - \frac{3\beta^2 - 11\beta + 8}{24 - 21\beta}, \quad (7)$$

and this allows us to write the stability condition in the following form:

$$\frac{3\Gamma_1 - 4}{4}\left(\frac{\mathrm{d}\log A}{\mathrm{d}\log\rho}\right)_{\rm env} < \frac{5 - 3\Gamma_1}{3}\left(\frac{\mathrm{d}\log\mu}{\mathrm{d}\log\rho}\right)_{\rm env}. \quad (8)$$

As the $\mathrm{d}\log\rho/\mathrm{d}\log m$ term is always negative throughout the star, we can rewrite the stability condition in a more convenient form:

$$\left(\frac{\mathrm{d}\log A}{\mathrm{d}\log m}\right)_{\rm env} > \frac{4}{3}\frac{(5/3) - \Gamma_1}{\Gamma_1 - (4/3)}\left(\frac{\mathrm{d}\log\mu}{\mathrm{d}\log m}\right)_{\rm env}. \quad (9)$$

In a star in which equation (9) is satisfied, a perturbed element will experience restoring forces that cause it to oscillate around its equilibrium position. It can be seen that in the limit of ideal gas ($\Gamma_1 = 5/3$), or when the composition is uniform, we recover the usual stability criteria $\mathrm{d}A/\mathrm{d}m > 0$. In the general case, however, A will typically increase outward, but can decrease in regions with an inverted composition gradient.

3 VALIDATION

3.1 Initial conditions

In the previous section we have presented a sorting algorithm that generates a collision product in hydrostatic equilibrium. As the method deals with non-rotating products, we validate it by carrying out simulations of head-on collisions between main-sequence stars of different mass and age. The full set of simulations is presented in Table 1.

Simulations of stellar collisions were carried out by means of a modified version of the GADGET2 code (Springel 2005). In particular, we included radiation pressure in the equation of state and the functionality which allows generation of relaxed models of parent stars in quasi-hydrostatic equilibrium (Lombardi et al. 2006; Turner et al. 1995).

We have prepared three-dimensional SPH stellar models from one-dimensional stellar models computed with the EZ stellar evolution code (Paxton 2004). In particular, we have used EZ to evolve a non-rotating zero age main-sequence (ZAMS) model with a primordial helium abundance $Y \simeq 0.3$ and metallicity $Z = 0.02$. The resulting star is composed of spherical mass-shells which store necessary stellar data, such as local composition, temperature and density, as well as enclosed stellar mass and radius. The stars are evolved until the primary star reaches its half-age of its main-sequence life-time (HAMS) or until the primary has only 1 per cent hydrogen abundance in its core (TAMS). In all cases the secondary star is evolved to the same age as the primary with which it collides.

3.2 Results

We have shown in Section 2 that the two main quantities which determine the structure of the collision product is buoyancy and composition. Because in main-sequence stars the mean molecular mass is mostly dependent on hydrogen mass fraction, we present in Fig. 1 buoyancy and hydrogen mass fraction profiles for a selection of the parent stars. In the case of TAMS stars, the primary consumed nearly all the hydrogen in its core. Nevertheless, the secondary has consumed less than the half of its initial hydrogen supply. HAMS parents, on the other hand, are barely evolved; all of the parent models have burnt less than the half of the initial amount of hydrogen in their cores.

The buoyancy of the parent stars is shown in the two lowest panels of Fig. 1. Even though the 20- and 40-$M_\odot$ stars are at the end of the main sequence, the buoyancy in their cores is noticeably higher than that of the secondary star. Therefore, based on the results of Section 2, it is natural to expect that the 8-$M_\odot$ star will occupy the centre of the merger product. In the case of the 10-$M_\odot$ primary, however, one may expect mixing, as the buoyancy of the primary and the secondary stars differ by less than a factor of 2, and this difference can be modified by shock heating.

In this work, we model shock heating by increasing the buoyancy of each fluid element. For this we need to assume a particular distribution of shock heating. Motivated by the results of Lombardi et al.

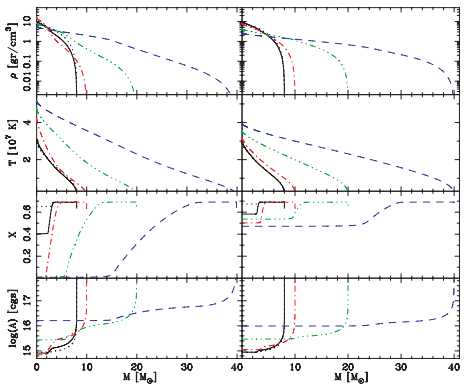

Figure 1. Internal structure of a selection of TAMS (left-hand side) and HAMS (right-hand side) parent stars which were used in simulations. The upper panels show density profile as a function of enclosed mass. The black solid and dotted lines on the left-hand side show density profile of the 8-$M_\odot$ star from T18 and T48 models respectively, while on the right-hand side the 8-$M_\odot$ star is taken from H18 and H48 models. The red dash–dotted, green dash–triple-dotted and blue dashed lines show density profiles of 10-, 20- and 40-$M_\odot$ stars, respectively. The second panels from the top show temperature profiles, while the third and fourth panels present hydrogen mass fraction and buoyancy profiles respectively.

(2002), we adopt the following simple distribution:

$$\log(A_{\rm f}/A_{\rm i}) = a + b\log(P_{\rm i}/P_{\rm c,i}). \quad (10)$$

Here, $A_{\rm i}$ and $A_{\rm f}$ are the initial and the final buoyancy of a fluid element, respectively, $P_{\rm i}$ is the initial pressure, and $P_{\rm c,i}$ is the central pressure of a parent star from which the fluid has come. We compute parameters a and b by fitting equation (10) to the simulation data.

One of the advantages of using equation (10) can be seen by looking at equation (3). As an SPH particle preserves its composition in the course of a simulation, equation (10) describes the change in entropy due to the shock heating process. This, in turn, potentially expands the range of applicability of the sorting algorithm presented in Section 2 to an arbitrary equation of state, such as of degenerate matter inside white dwarfs.

For every simulation from Table 1, we obtain a and b values in equation (10) for each of the parent stars. We use this equation to compute the change in the buoyancy for each of the mass shells of the parent stars, and then we apply the sorting algorithm to generate the structure of the collision product which we compare with the simulation results.

In Fig. 2 we present the results of the sorting algorithm and simulations. The sorting algorithm is able to reproduce two distinct branches in temperature, composition and buoyancy for TAMS collisions; the density, on the other hand, is single-valued as one would naturally expect. In the case of HAMS collisions, the branches are less pronounced, as expected, because the parent stars have roughly the same composition (see Fig. 1). A noticeable discrepancy in the density of the outer layers is caused by an inadequate representation of shock heating in these layers by equation (10); indeed, both the density and buoyancy of our simple model diverge from the SPH results at about the same enclosed mass. The mass loss in the collisions from Table 1 never exceeds 10 per cent: T18 (8.3 per cent), T28 (8.9 per cent), T48 (5.0 per cent), T88 (1.9 per cent), H18 (6.8 per cent), H28 (4.7 per cent), H48 (2.1 per cent), H88 (0.8 per cent), Z18 (6.4 per cent) and Z28 (4.5 per cent). As we expect, mass loss is less in collisions involving stars of significantly different mass, as less kinetic energy is redirected into the ejecta. In addition, we observe that mass loss is larger in collisions with evolved stars, due to their weakly bound envelopes.

We note that the very existence of two branches in the results of Fig. 2 means that the buoyancy A *does not* increase outward at all locations. In the case of model T18, it is actually the higher buoyancy branch, corresponding to hydrogen depleted fluid from the TAMS primary, which extends into the core of the merger product. Such a configuration is stable only because it is accompanied by a sufficiently steep gradient in composition. Indeed, in model H18, the parent stars are too young to yield large gradients in composition, and consequently it is the lower buoyancy fluid from the secondary that sinks to the centre of the merger product. It is also worth noting that in models Z18 and Z28, in which the ZAMS parent stars have uniform composition, we find that the buoyancy increases outwards throughout the collision products, as expected from equation (9).

As we increase the resolution of parent stars as treated by the sorting algorithm, adjacent mass shells in different branches become increasingly closely spaced. The resulting large gradients will eventually be smoothed by the microscopic mixing between neighbouring fluid elements. To simulate such mixing, we process the results from the sorting algorithm into equal-mass bins, such that each bin accommodates a sufficiently large number of mass shells. We then average the stellar data, such that the total volume and thermal energy of each bin, as well as the total mass of each of the

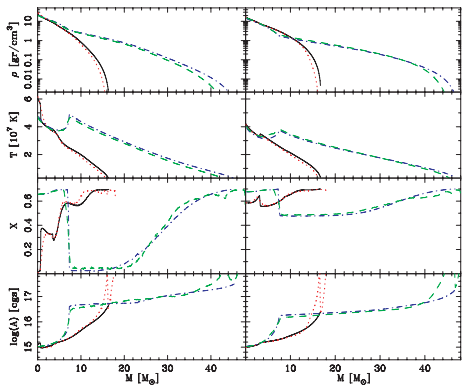

Figure 3. The structure of the mixed collision products from the same selection of models as presented in Fig. 2. Here, the black solid and red dotted lines show the results of the sorting algorithm and of the simulation, respectively, for the cases T18 on the left-hand side and H18 on the right-hand side. The blue dash–dotted and green dashed lines show the results of sorting algorithm and of the simulation respectively for the cases T48 on the left-hand side and H48 on the right-hand side. The upper panels show density profiles as a function of enclosed mass, and the second panel from the top shows temperature profiles. The third and the fourth panels from the top show hydrogen mass fraction and buoyancy profiles respectively.

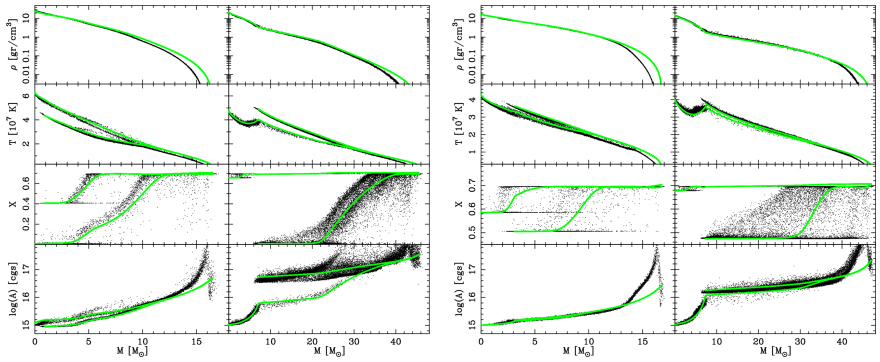

Figure 2. The non-mixed structure of the collision products from a selection of simulations. The left-hand set of plots displays results for TAMS collisions, whereas the right-hand set displays the same data for HAMS collisions. The black dots are the results of simulations, while the green circles are the results of the sorting algorithm. The upper panels show the density profile as a function of enclosed mass for T18, T48, H18 and H48 simulation models from left to right, respectively. In the second panels from the top, we show the temperature profile, and in the third and the fourth panels we show the hydrogen mass fraction and buoyancy profiles, respectively.

chemical elements, are conserved. From the average values of density, thermal energy and composition, we compute the rest of the thermodynamic quantities, such as temperature. We find that this procedure converges once the high resolution model has roughly 10^5 mass shells averaged into 200 bins. The simulation data is averaged in the same way.

In Fig. 3 we show the results of the mixing applied to the models shown in Fig. 2. Whereas no significant mixing occurs in models T48 and H48 as the 8-$M_\odot$ star settled in the centre of the primary, the interior of the collision product in model T18 is mixed. In model H18, however, only the core of the secondary star settles in the centre of the primary star; the rest of the fluid is mixed. The resulting buoyancy increases outwards throughout the product in all models, except in the very centre of T18. Here, the decrease in buoyancy at $\simeq 0.8\,M_\odot$ is accompanied by an increase in mean molecular mass in such a way that equation (9) is satisfied.

4 DISCUSSION AND CONCLUSIONS

We have presented a new sorting algorithm which generates the structure of collision products in hydrostatic equilibrium. We have tested the algorithm by carrying out a set of SPH simulations of head-on stellar collisions between massive main-sequence stars of different masses and ages. By calibrating the shock heating with the simulation data, we have been able to quickly generate the structure of the collision products consistent with the results of the simulations.

It takes less than a minute to generate a collision product for any of the models presented in Table 1, whereas an SPH simulations takes at least a day of CPU time on the same computer. Such an increase in speed will help to make it possible to include realistic stellar collisions in simulations of star clusters.

We have found that the chemical composition and temperature can be a multivalued function of the enclosed mass, if microscopic mixing processes are ignored. This is exhibited by the fact that the neighbouring mass shells have a discontinuously changing temperature and chemical composition, whereas the density and pressure remains continuous. Using the sorting algorithm, we have found that the situation is unaffected by increasing the number of shells. Instead, the chemical composition and temperature become double-valued in the continuous limit. Such an obviously unphysical situation is mended by microscopic mixing. We have simulated the mixing process by conservatively averaging multiple mass shells into a single mass bin. The resulted profiles are both single-valued and consistent with the simulation data.

We have found significant mixing in only the T18 and H18 models. The reason for this is that buoyancy in the core of the primary and the secondary stars are similar, whereas for the other models, such as T48 and H48, the buoyancy of the primary stars is substantially larger than that of the secondary stars. Therefore, in those cases, fluid from the secondary star occupies the central region of the collision product without being mixed with the fluid from the primary star. We therefore conclude that hydrodynamic mixing in collisions between main-sequence stars occurs only when the masses and ages of the parents stars are similar to each other. We find that mixing already becomes unimportant at the mass ratio $q \simeq 0.4$, which is the mass ratio of models T28, H28 and Z28. In such cases, the secondary star simply occupies the centre of the collision product without much mixing (Dale & Davies 2006; Suzuki et al. 2007).

Microscopic mixing may play an important role during the collision process itself. If the diffusion processes are ignored, the turbulent motion of the fluid can result in a discontinuous distribution of chemical composition and temperature, while maintaining continuity in density and pressure. Such a distribution is susceptible to microscopic mixing which tends to smooth the discontinuities (Dimotakis 2005). If the time-scale of microscopic mixing is larger than the time a collision product takes to settle into quasi-hydrostatic equilibrium, the mixing can be ignored during the collision event and applied only as a post-collision process. On the other hand, if the time-scale of the microscopic mixing is shorter than the time-scale of a collision event, then one must include the effects of mixing into the simulation itself.

The sorting algorithm can in principle be applied to any type of stars; for example, it is possible to apply it to the merger of white dwarfs. The basic requirement is simply to have the equation of state which gives the relationship between pressure, density, composition and specific entropy (or buoyancy), analogous to equations (3) and (4). While it is also necessary to determine mass loss and shock heating of the fluid, these can be estimated through energy conservation arguments.

ACKNOWLEDGMENTS

We thank Alexander Brown, Evert Glebbeek and Ujwal Kharel for useful discussions. We also acknowledge the use of the 3D virtual collaboration environment Qwaq Forums, which greatly sped up the remote collaboration leading to this Letter. The calculations for this work have been carried out on the LISA cluster, which is hosted by the SARA supercomputing centre. JCL is supported by the National Science Foundation under Grant No. 0703545, and EG and SPZ are supported by NWO (grants #635.000.303 and #643.200.503). This project was started during the Modest-7f workshop, which was hosted by the University of Amsterdam and supported by NOVA, NWO, LKBF and ASTROSIM grants.

REFERENCES

Clayton D. D., 1983, Principles of Stellar Evolution and Nucleosynthesis. Univ. Chicago Press, Chicago
Dale J. E., Davies M. B., 2006, MNRAS, 366, 1424
Dimotakis P. E., 2005, Ann. Rev. Fluid Mech., 37, 329
Freitag M., Gürkan M. A., Rasio F. A., 2006, MNRAS, 368, 141
Gaburov E., Gualandris A., Portegies Zwart S., 2007, MNRAS, submitted (arXiv:0707.0406)
Lombardi J. C., Thrall A. P., Deneva J. S., Fleming S. W., Grabowski P. E., 2003, MNRAS, 345, 762
Lombardi J. C., Jr, Proulx Z. F., Dooley K. L., Theriault E. M., Ivanova N., Rasio F. A., 2006, ApJ, 640, 441
Lombardi J. C., Jr, Rasio F. A., Shapiro S. L., 1996, ApJ, 468, 797
Lombardi J. C., Jr, Warren J. S., Rasio F. A., Sills A., Warren A. R., 2002, ApJ, 568, 939
Monaghan J. J., 2005, Rep. Progress Phys., 68, 1703
Paxton B., 2004, PASP, 116, 699
Portegies Zwart S. F., Baumgardt H., Hut P., Makino J., McMillan S. L. W., 2004, Nat, 428, 724
Portegies Zwart S. F., Makino J., McMillan S. L. W., Hut P., 1999, A&A, 348, 117
Sills A., Adams T., Davies M. B., Bate M. R., 2002, MNRAS, 332, 49
Springel V., 2005, MNRAS, 364, 1105
Suzuki T. K., Nakasato N., Baumgardt H., Ibukiyama A., Makino J., Ebisuzaki T., 2007, ApJ, 668, 435
Turner J. A., Chapman S. J., Bhattal A. S., Disney M. J., Pongracic H., Whitworth A. P., 1995, MNRAS, 277, 705

This paper has been typeset from a TEX/LATEX file prepared by the author.